
Developing Platinum-Group-Metal-Free Catalysts for Oxygen Reduction Reaction in Acid: Beyond the Single Metal Site

Qingying Jia (Primary Contact), Sanjeev Mukerjee
Northeastern University
360 Huntington Avenue
Boston, MA 02115
Phone: 617-373-5630
Email: q.jia@northeastern.edu

DOE Manager: Nancy Garland
Phone: 202-586-5673
Email: Nancy.Garland@ee.doe.gov

Contract No: DE-EE0008416

Subcontractor:
Lawrence Berkeley National Laboratory, Berkeley, CA

Project Start Date: January 1, 2019
Project End Date: December 31, 2020

Overall Objectives

- Develop durable and high-performance platinum group metal (PGM)-free catalysts and electrodes for automotive polymer electrolyte membrane fuel cells (PEMFCs).
- Understand the degradation mechanism of the M-N-C type of electrocatalysts upon long-term operation in PEMFCs.
- Realize the PGM-free catalysts with multiple metal centers (MMC).
- Model the PGM-free catalyst layer and explore limiting phenomena.

Fiscal Year (FY) 2019 Objectives

- Demonstrate PGM-free cathode electrode performance of 0.025 A/cm² at 0.90 V (iR-corrected) in a H₂/O₂ PEMFC (1.0 bar partial pressure, 80°C).
- Demonstrate the presence of MMC sites in synthesized M_x-N-C catalysts by high-angle annular dark-field and X-ray absorption spectroscopy (XAS)

Technical Barriers

This project addresses the following technical barriers from the Fuel Cell Technologies Office Multi-Year Research, Development, and Demonstration Plan¹:

- Durability
- Performance.

Technical Targets

The DOE technical targets and our current project status are listed in Table 1 for comparison.

This project is to develop M_(x)-N-C catalysts with dense MMC sites to meet the following the DOE 2025 activity target:

- 0.044 mA/cm² at 0.9 V_{IR-free}.

FY 2019 Accomplishments

- Developed a Fe-N-C PGM-free catalyst that delivers a current density of 0.033 mA/cm² at 0.9 V_{IR-free}, in a H₂/O₂ PEMFC (1.0 bar partial pressure, 80°C), exceeding our FY 2019 go/no-go target of 0.025 mA/cm² at 0.9 V_{IR} by 32%.
- Demonstrated the feasibility of non-contact pyrolysis in synthesizing active M-N-C catalysts.
- Revealed the thermal evolution pathway of the formation of the Fe-N₄ site during pyrolysis.
- Developed, coded, and exercised a continuum level model of transport phenomena within a PGM-free catalyst layer. The model demonstrated that local resistances combined with limited site density of the PGM-free catalyst can result in limiting currents and poor polarization performance. The model also gave design guidance for impact of electrochemical surface area and overall catalyst-layer thickness

¹ <https://www.energy.gov/eere/fuelcells/downloads/fuel-cell-technologies-office-multi-year-research-development-and-22>

Table 1. Technical Targets: Electrocatalysts for Transportation Applications

Characteristic	Units	DOE 2025 Electrocatalyst and MEA Targets	Project Status (5 cm ² cell)
Mass activity	A/mg _{PGM} @ 0.9 V _{IR-free}	≥0.044	0.033
MEA performance	mA/cm ² _{geo} @ 800 mV	≥300	220
Loss in initial catalytic activity (0.60–0.95 V cycling, 30k cycles)	% mass activity loss	<40	-
Loss in performance at 0.8 A/cm ² (0.60–0.95 V cycling, 30k cycles)	mV	≤30	-
Loss in performance at 1.5 A/cm ² (after carbon-corrosion test)	mV	<30	-

MEA – membrane electrode assembly

INTRODUCTION

Three major tasks were conducted in the first year of this project. The first one is to understand how the Fe-N₄ site forms during pyrolysis. In the 1980s, Yeager et al. [1] proved that pyrolyzing the mixture of M, N, and C precursors at elevated temperature can produce highly active M-N-C catalysts for the oxygen reduction reaction (ORR) in acidic media. Since then, highly active Fe-N-C catalysts have been produced by various methods such as those derived from polymer and organic compounds [2, 3] silica templating [4, 5](3, 4), and Zn-based metal organic framework (MOF) [6–9]. All these various methods carry the core feature of the pyrolysis route pioneered by Yeager et al. [1]: pyrolyzing the mixture of Fe, N, and C precursors in the temperature range of 900°–1,100°C, and they produce the same Fe-N₄ moieties that are commonly recognized as the active sites responsible for the high ORR activities of Fe-N-C catalysts in acid [2, 7, 10]. However, it is unclear how the Fe-N₄ site forms during pyrolysis. In collaboration with the ElectroCat consortium Advanced Photon Source led by Deborah Myers, who conducted the in-temperature X-ray absorption spectroscopy, we revealed the evolution pathway from Fe compounds to Fe-N₄ during pyrolysis. This fundamental understanding inspired a new synthesis route, the so-called non-contact pyrolysis wherein the Fe precursor is not in direct contact with N and C precursor during pyrolysis. The second task is to produce a high activity Fe-N-C catalyst by optimizing the non-contact pyrolysis. So far, we produced a Fe-N-C catalyst that delivers a current density of 0.033 mA/cm² at 0.9 V_{IR-free} in a H₂/O₂ PEMFC (1.0 bar partial pressure, 80°C), exceeding our FY 2019 go/no-go target of 0.025 mA/cm² at 0.9 V_{IR} by 32%. The third task is to develop a M_x-N-C catalyst with MMC sites via ionothermal carbonization that allows for the control over the pore size and distribution of the carbon matrix. While the presence of MMC sites is indicated by high-resolution transmission electron microscopy (HRTEM) and in situ XAS, it is inconclusive because of the co-presence of carbide that is partly electroactive and stable in acid. Because this group of catalysts did not exhibit exceptional ORR activity in a rotating disk electrode (RDE), far worse than that of the Fe-N-C synthesized via non-contact pyrolysis, we decided not to proceed further.

In the meantime, we have also worked on surface deposition methods including sputtering and ion beam assisted deposition to form M_x-N-C catalysts with MMC sites, with precursors containing pre-existing MMC sites.

APPROACH

The in-temperature XAS measurements during pyrolysis were performed at beamline 10-ID of the Materials Research Collaborative Access Team at the Advanced Photon Source, Argonne National Laboratory, to monitor the Fe site evolution during pyrolysis. The experimental apparatus for these experiments and the results of the first use of the apparatus to study the evolution of the Fe speciation during heat treatment of a Fe-doped zeolitic imidazolate framework (ZIF) is described in Myers et al. Three mixtures were subjected to in-

temperature XAS measurement. The powder precursors were loaded into a custom-built holder comprised of alumina tubes with inner diameters of 0.4 cm. A quantity of each powder needed to yield a Fe K-edge edge step of approximately 0.25 to 1 (0.09 to 0.3 mg Fe) was ball-milled for 2 hours for sufficient mixture and then packed into separate alumina tubes in the holder. The alumina tube holders were placed in the center of a quartz tube, equipped with gas and thermocouple ports and Kapton windows. A K-type thermocouple measured the temperature inside the quartz tube and was located just above the alumina tube sample holder. The quartz tube was placed in a clamshell furnace, mounted on a positioning platform. The beam was rastered over the sample holder by manipulating the position of the platform. Once the sample positions were fine-tuned, the quartz tube was purged with approximately 100 sccm flow of 99.995% helium, which had been passed through an oxygen trap. The Fe K-edge spectra were recorded in transmission mode and an iron foil spectrum was measured simultaneously with each sample spectrum for energy calibration. Transmission data were taken from 6.950 keV to 7.942 keV. Spectra were taken at room temperature, then the quartz tube was heated at a ramp rate of approximately 15°C/min under flowing helium to approximately the following temperature set points during the increasing temperature portion of the temperature profile: room temperature, 300°C, 400°C, 500°C, 600°C, 700°C, 800°C, 900°C, and 1,000°C. This was followed by controlled cooling to room temperature with temperature set points of 800°C, 600°C, 200°C, and room temperature at which spectra were acquired. Once the samples had cooled to room temperature, the helium flow was stopped, the quartz tube was opened to atmospheric air, and XAS scans were collected. Multiple XAS scans were collected at each temperature set point. The hold time at each temperature was approximately 15 minutes.

First is the Fe-MOF precursor with the synthesis following our previous protocol. Second is the mixture of $\text{FeCl}_2 \cdot 4\text{H}_2\text{O}$ and N-C. The N-C was synthesized by mixing 1,10-phenanthroline and ZIF-8 via ball milling, followed by pyrolyzing the mixture at 1,050°C in Ar and then at 900°C in NH_3 . The third one is the mixture of $\text{FeCl}_2 \cdot 4\text{H}_2\text{O}$ and SiO_2 . The Fe K-edge spectra were recorded in transmission mode. This was followed by controlled cooling to room temperature and then exposure to air at which spectra were acquired. The non-contact pyrolysis was conducted by placing N-C and Fe precursors separately in two boats in the furnace and then pyrolyzing in Ar. The boat containing the iron compound was located upstream in the Ar flow of the boat containing the N-C powder. The ORR performance of synthesized Fe-N-C catalysts was evaluated first in an RDE. The screened ones were evaluated in a PEMFC and characterized with multiple-component techniques including in situ XAS, HRTEM, Brunauer-Emmett-Teller, cavity ring down spectroscopy, and scanning electron microscopy to reveal their structures at the atomic level.

For the electrode modeling, a multiscale methodology was engaged that utilized continuum descriptions of transport of oxygen, electrons, and protons to the catalyst discrete sites, which is then upscaled using effectiveness factors to the thickness scale. The overall polarization performance is then predicted using well-established fuel-cell model and parameters.

RESULTS

The cyclic voltammogram (CV) and ORR polarization curve of the Fe-N-C catalyst optimized by RDE assessments are presented in Figure 1. The high capacitance as reflected by the broadness of the CV implicates the high electrochemical surface area of the catalyst. The redox peaks around 0.64 V arise from the $\text{Fe}^{3+/2+}$ redox transition. The high intensity of these peaks indicates relatively abundant Fe-N₄ sites that are electroactive. These results in combination suggest abundant Fe-N₄ sites anchored onto porous carbon matrix, which represents a desired morphology for this type of ORR catalyst. Indeed, the ORR polarization curve shows a half wave potential of 0.82 V (all potentials are versus reversible hydrogen electrode), and a limiting current of 4.0 mA/cm² with a rotation rate of 900 rpm. This ORR performance in an RDE is comparable to the state of the art. This catalyst was then sent to Giner, Inc. for PEMFC testing. The MEA has a size of 5 cm². It is composed of an anode of Pt/C (TKK, 47.2%), a membrane of Nafion 212, and a cathode with the Fe-N-C catalyst with a loading of 6 mg·cm². Details of the PEMFC testing are given in the caption of Figure 1. The polarization curve present in Figure 1 is the first one collected from the high potential to low potential (cathodic scan). The current density at 0.9 V is 0.033 A·cm⁻² and 0.028 A·cm⁻² with and without iR correction, respectively (Figure 1d). This activity surpasses our proposed first year go/no-go value of 0.025 A·cm⁻² at 0.90 V (iR-corrected) in a H₂/O₂ PEMFC by one-third and is very close to the end of project goal of 0.035 A·cm⁻² at

0.90 V (iR-corrected) in a H₂/O₂ PEMFC. It is also superior to any published results based on PGM-free samples in a PEMFC by far. The current density at 0.8 V is 0.38 A·cm⁻² and 0.22 A·cm⁻² with and without iR correction, respectively (Figure 2c).

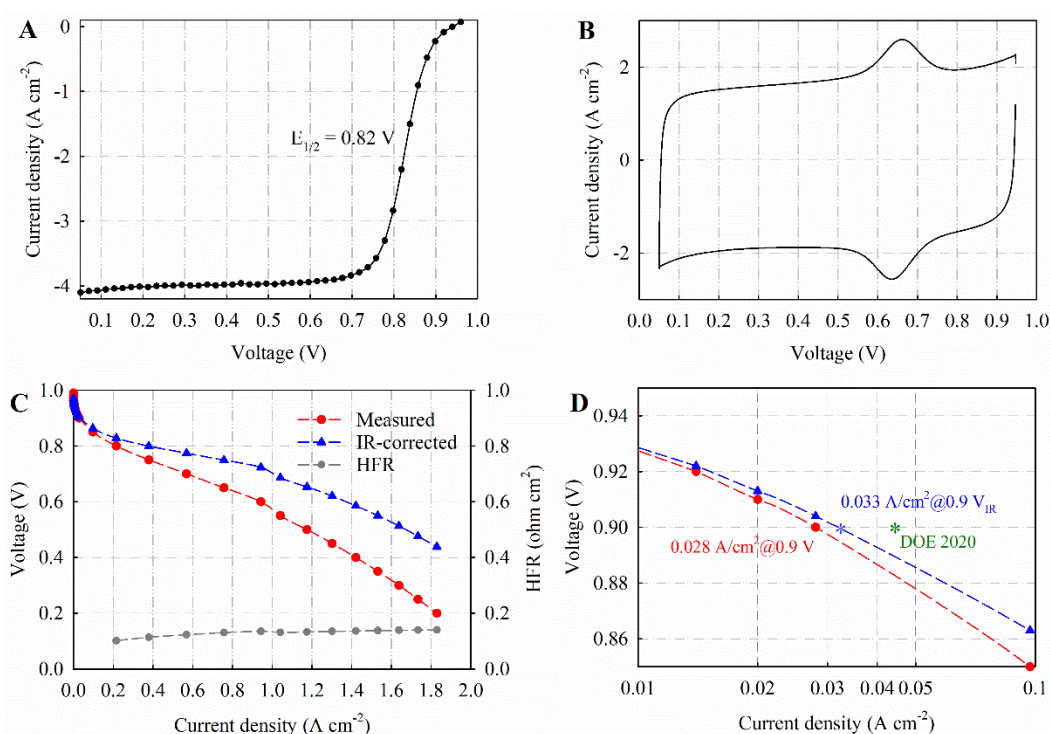


Figure 1. (a) ORR performance of the catalyst. Steady-state RDE polarization plot was obtained by using a 20-mV potential step and 25-s potential hold time at every step in O₂-saturated 0.5 M H₂SO₄ from 0.05 to 0.95 V with a rotation rate of 900 rpm at room temperature. (b) CV of the same catalyst was obtained after the ORR polarization curve present in (a) in the same electrolyte with a scan rate of 10 mVs⁻¹ at room-temperature. (c) H₂-O₂ PEMFC polarization curves with and without IR-correction. Cathode: ~6.0 mgcm⁻² of the catalyst; anode: 0.3 mg_{Pt}·cm⁻² Pt/C; membrane: Nafion 212; 200-mL/min⁻¹ gas fed at both anode (H₂) and cathode (O₂) with 100% RH and 1.0 bar partial pressure each side; cell 80 °C; electrode area 5 cm². (d) The Tafel plot derived from the IR-corrected ORR polarization curve displayed in (c) to manifest the activity at 0.9 V in comparison with DOE 2020 target.

A second Fe-N-C catalyst was recently synthesized for RDE and H₂-air PEMFC testing (Figure 2). This catalyst exhibits better ORR kinetics but lower limiting current and capacitance compared to the Fe-N-C catalyst shown above. This means that this catalyst may have even more Fe-N₄ sites, but it also contains inorganic Fe species that block the pores and graphitize the carbon during pyrolysis. In a H₂-air PEMFC, it delivers a maximum power density of 0.34 W/cm². This performance is slightly lower than the state-of-the-art performance of ~0.4 W/cm² obtained with a PGM-free catalyst tested under the same conditions [2]. The rapid drop of the current below 0.6 V indicates poor mass transport of this catalyst, which appears to be consistent with the RDE results. This rapid drop at high current region dramatically reduces the power density of the catalyst. Based on these understandings, we concluded that one of the key factors of non-contact pyrolysis that limits the PEMFC performance of the two catalysts may be the morphology of the NC that limits the Fe-N₄ site density and the mass transport. It may also lead to selective formation of inorganic species if the N-doped microporous defects are not enough to capture single Fe atoms to form Fe-N₄ sites. Preliminary TEM results do show that the NC has some extent of agglomeration. Based on the hypothesis, our ongoing and future efforts are optimizing the NC catalyst.

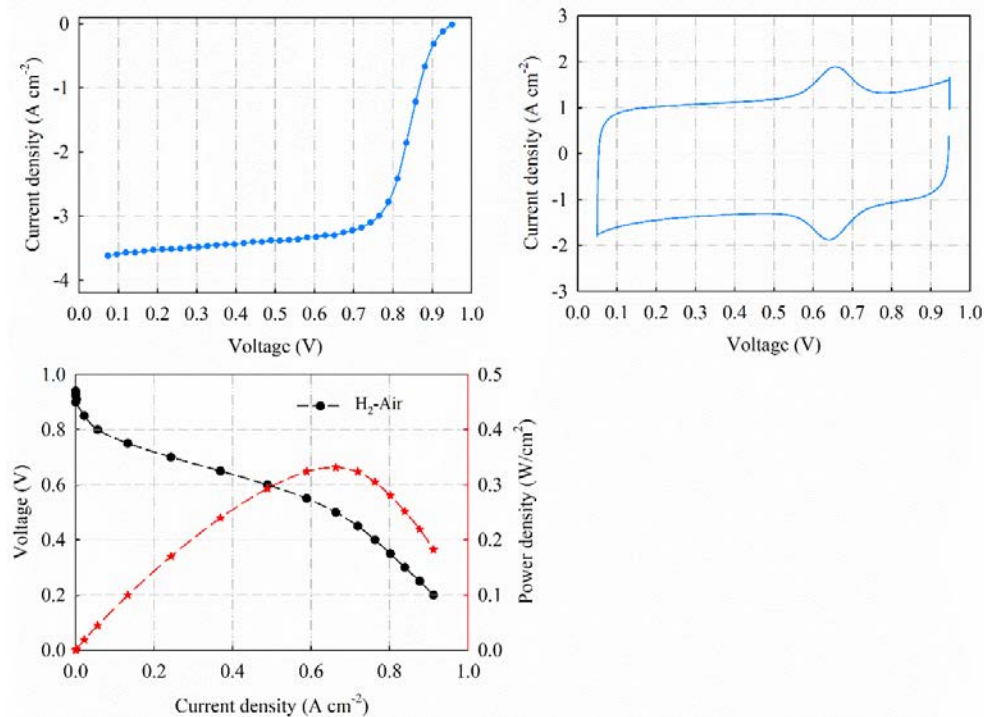


Figure 2. (a) ORR performance of the catalyst. Steady-state RDE polarization plot was obtained by using a 20-mV potential step and 25-s potential hold time at every step in O₂-saturated 0.5 M H₂SO₄ from 0.05 to 0.95 V with a rotation rate of 900 rpm at room temperature. (b) CV of the same catalyst was obtained after the ORR polarization curve present in (a) in the same electrolyte with a scan rate of 10 mVs⁻¹ at room-temperature. (c) H₂-air fuel cell polarization plots. Cathode: ~4.0 mg_{Pt}·cm⁻² of Fe-N-C, air 200 mL·min⁻¹; 100% relative humidity (RH); and 1.0 bar partial pressure. Anode: 3.0 mg_{Pt}·cm⁻² Pt/C; H₂ 200 mL·min⁻¹; 100% RH; and 1.0 bar partial pressure. Membrane Nafion 212, cell 80 °C, electrode area 5 cm².

By optimizing the synthesis process of the NC, we produced a new NC moiety that possesses ultra-high capacitance as reflected by the CV (not shown). As a result, the new Fe-N-C catalyst exhibits a half wave potential of 0.85 V (Figure 3a), meeting our milestone. It also exhibits a limiting current density of 3.9 mA/cm², comparable to the first Fe-N-C sample synthesized with the previous NC moiety. In addition, the synthesized Fe-N-C catalysts possess an extraordinarily high capacitance as manifested by the high broadness of the CV, as well as abundant electrochemical active Fe-N₄ sites as reflected by the prominent Fe-redox peaks around 0.64 V (Figure 3b). This catalyst will be subject to PEMFC evaluation next.

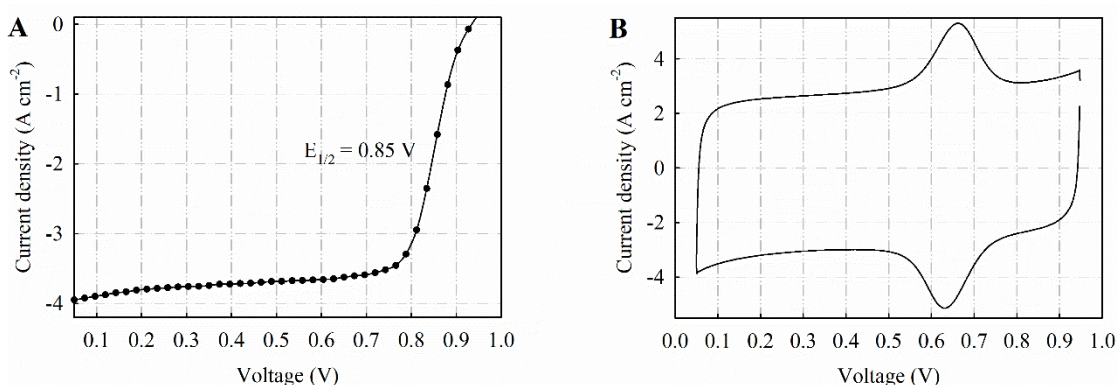


Figure 3. (a) ORR performance of the catalyst. Steady-state RDE polarization plot was obtained by using a 20-mV potential step and 25-s potential hold time at every step in O₂-saturated 0.5 M H₂SO₄ from 0.05 to 0.95 V with a rotation rate of 900 rpm at room temperature. (b) CV of the same catalyst was obtained after the ORR polarization curve present in (a) in the same electrolyte with a scan rate of 10 mVs⁻¹ at room-temperature.

A multi-scale approach is used to analyze the effect of catalyst-ionomer interaction. First, a microscale analysis is performed on an agglomerate model. Using specific catalyst sites (denoted by white in Figure 4a) and a local or thin-film resistance derived from the interaction of the ionomer with the catalyst, Figure 4a shows the oxygen partial pressure profile. The oxygen pressure changes significantly, and the core of the agglomerate is mostly oxygen starved due to lower permeability. This value is then used to determine the effectiveness factor of the agglomerate as shown in Figure 4b. As seen, these resistances result in poor utilization of the catalyst, which exacerbates the local resistances due to the low catalyst site density. Finally, the impacts on polarization can be seen in Figure 4c, where the use of thin-film properties reduces cell performance at higher currents and oxygen transport becomes critical, mimicking the local resistance effects seen in PGM catalyst layers with low PGM loading. Overall, it is seen that ionomer-catalyst interactions can significantly affect fuel cell performance at both the micro and macroscale.

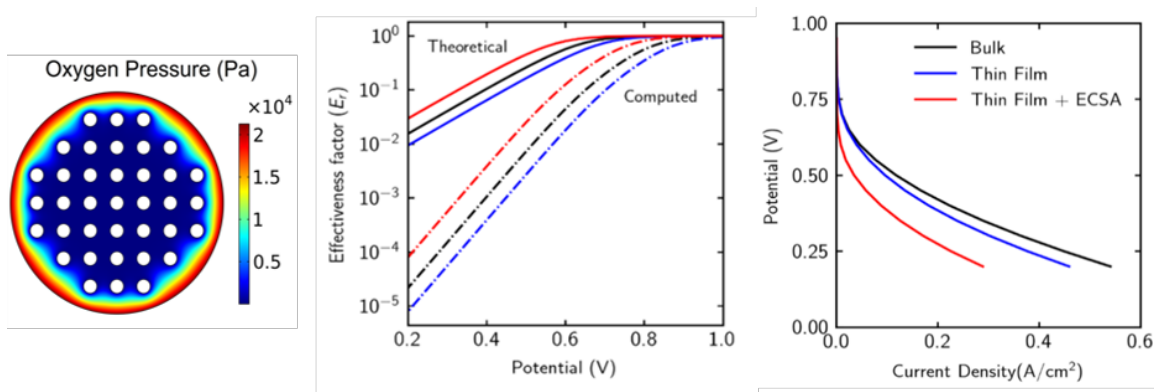


Figure 4. (a) Oxygen partial-pressure distribution in agglomerate at 40% RH and 0.2 V, where the white spots are the catalyst sites. (b) Agglomerate effectiveness factors at 90% RH for different agglomerate properties, where the solid lines show theoretical values and dotted lines show computed values. (c) Macroscale fuel cell performance at 90% RH.

CONCLUSIONS AND UPCOMING ACTIVITIES

We first revealed the Fe-N₄ site evolution pathway during synthesis and pointed out the possible existence of gas-phase single Fe atoms during the pyrolysis. Based on this hypothesis, we demonstrated the feasibility of non-contact pyrolysis. We then produced a Fe-N-C catalyst via non-contact pyrolysis that delivers a current density of 0.033 mA/cm² at 0.9 V_{IR-free} in a H₂/O₂ PEMFC (1.0 bar partial pressure, 80°C), exceeding our FY 2019 go/no-go target of 0.025 mA/cm² at 0.9 V_{IR}. Next, we will further optimize the non-contact pyrolysis aiming to meet the DOE 2020 activity target of 0.044 mA/cm² at 0.9 V_{IR}. We will also transfer the knowledge and experience gained from the non-contact pyrolysis to synthesize M_x-N-C catalysts with MMC sites.

An initial model was developed for the PGM-free catalyst layers showing mass-transport issues engendered by having limited reaction sites (increased impact of local resistance, thicker catalyst layer, etc.). Future work will focus on model agreement between measured and simulated polarization curves with a focus on accurate capture of the issues of ionomer adsorption onto the reaction sites and water management at higher RH due to the limited number of reaction sites within the PGM-free catalyst layer.

SPECIAL RECOGNITIONS AND AWARDS/PATENTS ISSUED

1. We submitted a patent application for non-contact pyrolysis, which is under internal review by Northeastern University.

FY 2019 PUBLICATIONS/PRESENTATIONS

2. J. Li, L. Jiao, M.-T. Sougrati, S. Mukerjee, E.C. Wegener, A.J. Kropf, D.J. Myers, F. Jaouen, and Q. Jia, *Meeting Abstracts MA2019-02* (2019): 1610.
3. L. Jiao, E. Liu, L. Richard, S. Mukerjee, and Q. Jia, *Meeting Abstracts MA2019-02* (2019): 999.
4. L. LaRochelle Richard, Q. Jia, and S. Mukerjee, *Meeting Abstracts MA2019-01* (2019): 640.

5. Q. Jia, J. Li, D.J. Myers, A.J. Kropf, and S. Mukerjee (Invited), *Meeting Abstracts* MA2019-01 (2019): 1485.
6. J. Li, L. Jiao, E. Wegener, L. Richard, E. Liu, A. Zitolo, M. Sougrati, S. Mukerjee, Z. Zhao, Y. Huang, A. Kropf, F. Jaouen, D. Myers, and Q. Jia, “The Evolution Pathway from Iron Compounds to Fe₁(II)-N₄ sites through gas-Phase iron During Pyrolysis,” Submitted to *J. Am. Chem. Soc.*

REFERENCES

1. S. Gupta, D. Tryk, I. Bae, W. Aldred, and E. Yeager, *J. Appl. Electrochem.* 19 (1989): 19-27.
2. H.T. Chung, D.A. Cullen, D. Higgins, B.T. Sneed, E.F. Holby, K.L. More, and P. Zelenay, *Science* 357 (2017): 479-484.
3. U. Tylus, Q. Jia, K. Strickland, N. Ramaswamy, A. Serov, P. Atanassov, and S. Mukerjee, *J. Phys. Chem. C* 118 (2014): 8999-9008.
4. A. Serov, K. Artyushkova, E. Niangar, C. Wang, N. Dale, F. Jaouen, M.-T. Sougrati, Q. Jia, S. Mukerjee, and P. Atanassov, *Nano Energy* 16 (2015): 293-300.
5. X. Wan, X. Liu, Y. Li, R. Yu, L. Zheng, W. Yan, H. Wang, M. Xu, and J. Shui, *Nature Catalysis* 2 (2019): 259-268.
6. E. Proietti, F. Jaouen, M. Lefèvre, N. Larouche, J. Tian, J. Herranz, and J.-P. Dodelet, *Nat. Commun.* 2 (2011): 416.
7. J. Li, S. Ghoshal, W. Liang, M.-T. Sougrati, F. Jaouen, B. Halevi, S. McKinney, G. McCool, C. Ma, X. Yuan, Z.-F. Ma, S. Mukerjee, and Q. Jia, *Energy Environ. Sci.* 9 (2016): 2418-2432.
8. H. Zhang, S. Hwang, M. Wang, Z. Feng, S. Karakalos, L. Luo, Z. Qiao, X. Xie, C. Wang, D. Su, Y. Shao, and G. Wu, *J. Am. Chem. Soc.* 139 (2017): 14143-14149.
9. H. Zhang, H.T. Chung, D.A. Cullen, S. Wagner, U.I. Kramm, K.L. More, P. Zelenay, and G. Wu, *Energy Environ. Sci.* 12 (2019): 2548-2558.
10. A. Zitolo, N. Ranjbar-Sahraie, T. Mineva, J. Li, Q. Jia, S. Stamatina, G.F. Harrington, S.M. Lyth, P. Krttil, S. Mukerjee, E. Fonda, and F. Jaouen, *Nat. Commun.* 8 (2017): 957.